Single-nanorod plasmon nanolaser: A route toward a three-dimensional ultraconfined lasing mode

Yixiao Gao,[1] Hao Wu,[1] Ning Zhou,[1] Yuxin Yang,[1] Xin Guo,[1] Pan Wang,[1] Jianqiang You [2] Ying Gu [3] Guowei Lu [3] Qihuang Gong,[3,4] and Limin Tong [1,4,*]

[1]*Interdisciplinary Center for Quantum Information, State Key Laboratory of Modern Optical Instrumentation, College of Optical Science and Engineering, Zhejiang University, Hangzhou 310027, China*

[2]*Interdisciplinary Center for Quantum Information, Department of Physics, Zhejiang University, Hangzhou 310027, China*

[3]*State Key Laboratory for Mesoscopic Physics, Frontiers Science Center for Nano-optoelectronics and Collaborative Innovation Center of Quantum Matter, School of Physics, Peking University, Beijing 100871, China*

[4]*Collaborative Innovation Center of Extreme Optics, Shanxi University, Taiyuan 030006, China*

A single-nanoparticle plasmon laser with ultratight optical confinement in all three dimensions is a long-cherished but yet to be realized goal. Here we propose an experimentally realizable plasmon laser using a single nanorod. We show that, by harnessing a Au-nanorod cavity with a large gain from a Purcell-enhanced stimulated emission rate and greatly suppressed high-order mode dissipation, it is possible to implement a dipole-mode plasmon laser with accessible material parameters. Our approach may lead to a real single-nanoparticle plasmon laser with three-dimensional ultraconfinement and offers an opportunity to explore and utilize the enhanced light-matter interaction at a lower dimension.

I. INTRODUCTION

Nanoscale plasmon lasers relying on surface plasmon amplification by stimulated emission [1] can offer an ultraconfined coherent light field to significantly enhance the light-matter interaction and are vital for a variety of applications from ultrasensitive sensing, spectroscopy, and nonlinear optics to next-generation ultrafast on-chip sources [2,3]. Since their first proposal in 2003 [1], one- (1D) and two-dimensional (2D) ultraconfined plasmonic lasing modes have been experimentally obtained in a number of 2D and 1D plasmonic nanosystems [4–7] and have shown extraordinary advantages of compact mode volume, low power consumption, and ultrafast modulation speed [3]. However, three-dimensional (3D) ultraconfined lasing systems, which are one of the ultimate goals of plasmon lasers [8] and are mostly supposed to be achieved with zero-dimensional plasmonic nanoparticles [1,9], have not yet been convincingly realized [10]. In the past decade, some experimental results on nanoparticle plasmon lasers have been reported [11,12], but there has been significant debate [13] on whether the lasing signal really comes from a single-nanoparticle cavity mode due to the requirement of unrealistically high gain or pump intensity [14–16]. Now it is becoming more and more clear that they are loosely confined random lasers or the like rather than single-nanoparticle plasmon lasers, as the gain required for reaching the single-nanoparticle lasing threshold under those conditions is experimentally inaccessible [10,17]. Here we propose a single-nanorod plasmon laser that is realistically achievable. Based on the theoretical calculation with

semiclassical rate equations, we find that a single-nanoparticle plasmon laser is possible only when the gain is significantly enlarged via a Purcell-enhanced stimulated emission rate and the high-order mode dissipation is effectively suppressed, which can be achieved in a single-nanorod system. More specifically, we use a Au nanorod with the same diameter (14 nm) as the Au nanosphere in a previous attempt [11], which is a slightly elongated nanoparticle but still retains the 3D ultrahigh confinement. We show that it is possible to reduce the dipole-mode lasing threshold to an attainable level, with a mode volume down to 1.3 times that of a nanosphere. It is worth mentioning that, previously, without considering the Purcell effect, plasmon amplification from gain-assisted gold nanorods with larger sizes has been studied theoretically [18]. Here we investigate the establishment and dynamical evolution of the lasing oscillation in a gain-coupled single-nanorod system on much lower dimensions and show that Purcell-enhanced stimulated emission plays a crucial role in determining the lasing threshold in such ultraconfined systems.

II. THEORETICAL MODEL

Our theoretical model of the single-nanorod plasmon laser is schematically illustrated in Fig. 1. A Au nanorod, whose permittivity is described by a Drude model (Appendix A), is wrapped by an active layer containing gain molecules (e.g., a silica substrate doped with uniformly distributed fluorescent gain molecules [10], about 15 nm in thickness). A 1-nm-thick gain-free isolation layer covering the entire surface of the nanorod is a spacer layer for reducing the quenching of the molecules [19]. The gain property and the dynamic evolution of the plasmon number in the nanorod-coupled fluorescent
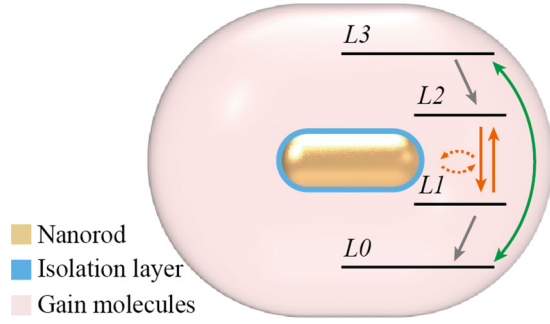
*phytong@zju.edu.cn

FIG. 1. Schematic of a Au nanorod coated by gain molecules described by a four-level system. The stimulated emission rate from upper level 2 (*L2*) to lower level 1 (*L1*) can be significantly enhanced via the Purcell effect with the presence of ultraconfined LSPR modes in the Au nanorod.
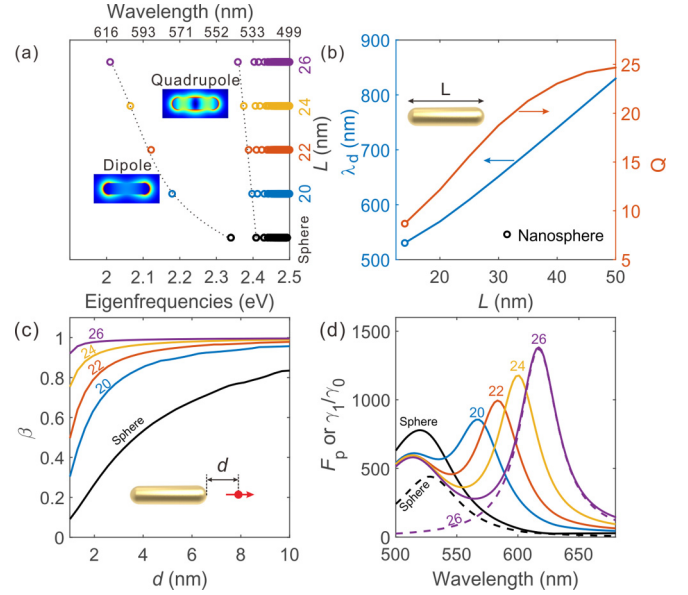

FIG. 2. (a) Resonant wavelengths of eigenmodes of four nanorods and a 14-nm-diameter nanosphere embedded in silica with a refractive index of 1.46. All nanorods have the same diameter d of 14 nm but different lengths L of 20, 22, 24, and 26 nm. (b) Resonant wavelength and quality factor of the dipole mode in a 14-nm-diameter nanorod with different L. (c) β factor as a function of the emitter-nanoparticle separation d. The emitter is positioned with its dipole moment along the nanorod axis, as shown in the inset. (d) Wavelength-dependent F_P (solid lines) and γ_1 (dashed lines). The emitter-nanoparticle separation is 5 nm. The length of each nanorod is labeled next to the corresponding curve in nanometers.

molecule system are described by a four-level system governed by semiclassical rate equations. The total spontaneous decay rate of the fluorescent emitter (*L2* to *L1*) is influenced by the local density of states and can be obtained by using the dyadic Green's function [20]

$$\gamma_{\text{tot}} = \frac{2}{\hbar} \text{Im}(\mathbf{p}^* \cdot \mathbf{E}), \quad (1)$$

where $\mathbf{E}$ is the local electric field and $\mathbf{p}$ is the dipole moment of the radiative transition from level 2 to level 1 that is randomly oriented in the fluorescent emitters. This means that the emitter decay rate depends on the relative orientation between the dipole moment and the direction of the electric field, and the large field gradient of the ultraconfined localized surface plasmonic resonance (LSPR) in a nanorod can give rise to a highly position dependent emitter decay rate. The radiative decay could be coupled to multiple LSPR modes. To calculate the contribution of a certain LSPR mode to the radiative decay, we employ the quasinormal-mode expansion formalism by expanding the total field $\mathbf{E}$ as a superposition of lossy plasmonic eigenmodes of a nanorod [21],

$$\mathbf{E} = \Sigma \eta_m \mathbf{E}_m, \quad (2)$$

where the expansion coefficient $\eta_m = \omega \mathbf{p} \cdot \mathbf{E}_m / (\omega_m - \omega)$, $\mathbf{E}_m$ is the normalized complex electric field of the mth-order LSPR eigenmode (e.g., $m = 1$ for the dipole mode) with a complex eigenfrequency of ω_m, and ω is the radiative transition frequency of emitters. Thus, the rate of decay into the mth-order mode is $\gamma_m = 2\eta_m \mathbf{p} \cdot \mathbf{E}_m / \hbar$. For a certain emitter located within the near field of LSPR of the nanorod, the ratio of decay into the dipole mode (i.e., the β factor) can be obtained as $\beta = \gamma_1/\gamma_{\text{tot}}$. It is worth noting that, in a plasmonic nanocavity, β and γ_m are position dependent due to the inhomogeneous spatial distribution of the field intensity (Appendix B). Also, an emitter within the near field of LSPR may also radiate into free space. However, in the model studied here, all emitters are located in close vicinity to the nanorod (e.g., <15 nm in separation), owing to the large Purcell effect F_P, e.g., $F_P > 500$; the majority of the decay energy is channeled into the LSPR modes of the nanorod, and those coupled to free space can be neglected. In addition, we assume the emitter-coupled highly lossy system (e.g., cavity

lifetime on the 10-fs level) operates in the weak-coupling regime [8], and the quantum effects on the nanorod properties (e.g., permittivity) are neglectable since the feature size of the nanorod considered here is larger than 10 nm [22].

III. RESULTS AND DISCUSSION

A. Modal characteristics in a nanorod system

The immediate advantages of using a nanorod instead of a nanosphere as a nanocavity for plasmonic lasing oscillation lie in three aspects: first, elongating a nanosphere into a nanorod significantly increases the spectral separation Ω between the dipole mode and the quadrupole mode (or other higher-order modes), which is crucial to suppress the energy dissipation via higher-order LSPR modes and channel a larger fraction of transition energy (*L2* to *L1*) into the lasing mode (i.e., the dipole mode of the nanorod). Figure 2(a) gives the calculated LSPR eigenfrequencies of five gold nanoparticles (four nanorods and one nanosphere), which are all 14 nm in diameter and embedded in silica. Compared to the relatively small Ω (15 nm) of a nanosphere that is not large enough to exclude the quadrupole and higher-order modes from the effective gain spectrum (usually around 50 nm [23]) centered at the peak wavelength of the dipole-mode LSPR, the Ω of a nanorod increases with the nanorod length L and is large enough (e.g., 91 nm in a 26-nm-long nanorod) to suppress the energy dissipation via high-order LSPR modes

whose coupling efficiency is proportional to $1/\Omega$. Second, elongating a nanosphere to a nanorod increases the mode volume and redshifts the LSPR of the dipole mode [Fig. 2(b)], which leads to a significant increase in the Q factor of the plasmonic nanocavity, defined as $\mathrm{Re}(\omega_m)/[2\mathrm{Im}(\omega_m)]$. For reference, Q increases from 8.7 for a nanosphere to 16.3 for a 26-nm-long nanorod. Thus, compared to a nanosphere cavity, a nanorod cavity can effectively suppress the higher-order mode-coupling channel and increase Q of the dipole LSPR mode, enabling a much higher fractional radiative decay into the dipole lasing mode. As an exemplary case shown in Fig. 2(c), with emitters located at a distance of $d = 1$ nm from the apex of the nanoparticle (nanorod/nanosphere), β is small (about 0.09) for a nanosphere but greatly enhanced in a nanorod system (e.g., 0.92 in the 26-nm-long nanorod). For $d > 2$ nm, in a nanorod system, β is larger than 0.9 (approaching 1.0 when $d > 5$ nm); however, in a nanosphere system, β is, on average, below 0.6. Meanwhile, for the dipole mode, β decreases quickly when $d < 1$ nm, indicating the increase in coupling transition energy into higher-order modes. Therefore, in the nanoparticle-based plasmon lasing system discussed here (i.e., illustrated in Fig. 1), Fig. 2(c) clearly shows that a 1-nm spacer is necessary not only for avoiding the quenching of the fluorescent molecule emitters [19,23] but also for efficiently suppressing the dissipation via higher-order LSPR modes (whose lasing thresholds are typically much higher than the dipole mode), similar to that in nanosphere systems reported previously [24]. Finally, compared to a nanosphere, a nanorod with the same diameter but larger length can effectively couple to more fluorescent molecules, which is critical to offer higher gain (under sufficiently large pump intensity and/or Purcell enhancement) in high-loss plasmonic nanocavities. In addition, besides the larger number of available gain molecules, the suppressed high-order mode dissipation and the higher Q of the dipole mode are also beneficial to Purcell enhancement of the stimulated emission rate and thus the effective gain for building up dipole-mode lasing oscillation.

To evaluate the Purcell effect, as an example, Fig. 2(d) gives the calculated F_P (i.e., the normalized decay rate $\gamma_{\mathrm{tot}}/\gamma_0$) of a dipole emitter placed 5 nm away from the apex of the nanorod, where γ_0 is the free-space decay rate of the emitter embedded in SiO$_2$. It shows that, for a nanorod with the same L, the peak value of F_P occurs around the central wavelength of the dipole mode in Fig. 2(b) and can be larger than 10^3 when $L > 22$ nm, much larger than that of a nanosphere with the same diameter. Also, the peak value of F_P increases with L due to the redshifted resonant wavelength and higher cavity Q factor [Fig. 2(b)].

It should be noted that although we show only a typical emitter-nanoparticle configuration as an example, most cases of emitter-nanoparticle coupling behave similarly. Also, the large mode separation in a longer nanorod would make emitters coupled to the lasing dipole mode more efficient.

B. Lasing dynamics with Purcell-enhanced gain

Next, we consider a typical nanorod plasmon laser system with a dipole-mode resonant wavelength of 651 nm and Q of 18.38 (corresponding to a 14-nm-diameter 30-nm-long

nanorod, with a mode lifetime of $\tau = Q/\omega = 6.35$ fs) and assume a free-space decay rate γ_0 of 1×10^8 s^{-1} for fluorescent molecules in the gain material [23]. The semiclassical rate equations for a nanorod plasmon laser system can then be obtained from a nanoparticle system [10] and expressed as

$$\frac{dn}{dt} = N_2\gamma_1 + (N_2 - N_1)\gamma_1 n - n\omega/Q,$$

$$\frac{dN_0}{dt} = (N_3 - N_0)\gamma_{\mathrm{p}} + N_1\gamma_{10},$$

$$\frac{dN_1}{dt} = (N_2 - N_1)\gamma_1 n + N_2\gamma_{\mathrm{tot}} - N_1\gamma_{10}, \qquad (3)$$

$$\frac{dN_2}{dt} = (N_1 - N_2)\gamma_1 n - N_2\gamma_{\mathrm{tot}} + N_3\gamma_{32},$$

$$\frac{dN_3}{dt} = (N_0 - N_3)\gamma_{\mathrm{p}} - N_3\gamma_{32},$$

where n is the plasmon number in the lasing dipole mode, N_i is the population at level i ($i = 0$, 1, 2, and 3), γ_{p} is the pump rate, the nonradiative interband transition rates γ_{32} and γ_{10} (from level 3 to level 2 and level 1 to level 0) are assumed to be 1×10^{13} s^{-1} [10], and γ_1 is the rate of fluorescent molecule decay into the dipole plasmon mode. For simplicity and phenomenological illustration, we assume that the emitters are uniformly distributed in the gain medium with a total number of $N_{\mathrm{tot}} = \Sigma_0^3 N_i = 3000$ and have an average β of 0.9. The pump light is assumed to be 1-ps-long Gaussian pulses with a peak pump rate of 1×10^{12} s^{-1}, corresponding to 532-nm-wavelength pump pulses with a peak intensity of 4.67 GW/cm^2 or an average power of 0.11 nW on the cross section of the nanolaser considered here at a repetition rate of 1 kHz (see Appendix D).

With the reasonable assumption that the initial populations of both levels N_1 and N_2 are zero and the total decay rate γ_{tot} is contributed mainly by the radiative decay (i.e., an internal quantum efficiency approaching 100%), the calculated temporary evolution of the dipole-mode plasmon number n is given in Fig. 3(a), in which the evolution behavior can be categorized into four regions by the decay rate γ_{tot}:

(i) At small γ_{tot}, e.g., $\gamma_{\mathrm{tot}} = 1 \times 10^{10}$ s^{-1}, corresponding to $F_P = 100$, the population inversion ratio (PIR), measured as $(N_2 - N_1)/N_{\mathrm{tot}}$, increases almost simultaneously upon the arrival of the pump pulse until it reaches a saturated value of about 67% around 4 ps, which is a clear signature of population inversion. However, due to the small γ_{tot} that offers insufficient seed photons (here the dipole-mode plasmons) for stimulated emission, gain from the stimulated emission cannot compensate the cavity loss, hindering the buildup of the laser oscillation. The unreached lasing state is also confirmed by the very low plasmon number ($n < 1$) throughout the process.

(ii) When γ_{tot} increases to exceed a certain threshold [the onset point in Fig. 3(a), corresponding to a level of $\gamma_{\mathrm{tot}} = 6.3 \times 10^{10}$ s^{-1}, as denoted by the red dashed line], e.g., $\gamma_{\mathrm{tot}} = 3.2 \times 10^{11}$ s^{-1}, corresponding to $F_P = 3.2 \times 10^3$, the significantly Purcell enhanced spontaneous and stimulated emission accelerates the decay rate from lasing level $L2$ to $L1$, resulting in a reduced PIR (e.g., peak PIR drops down to about 15%) compared to that in case (i), although large enough to ensure population inversion. At the same time, the enhanced spontaneous emission boosts the stimulated emission [25–27],
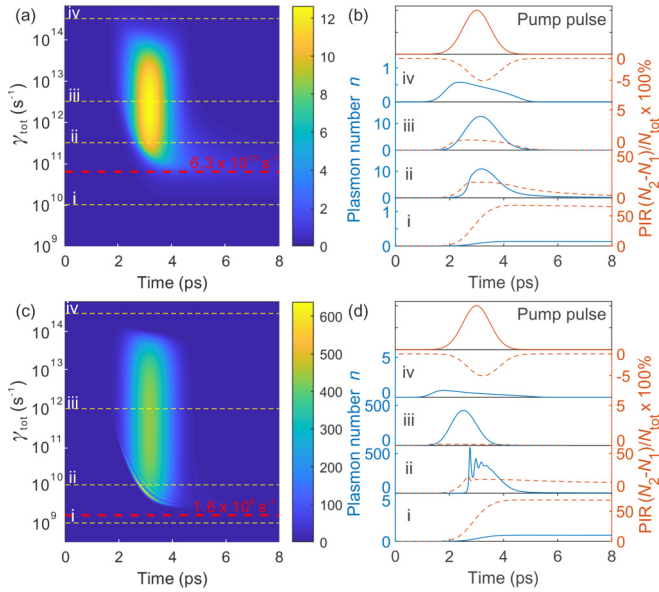
FIG. 3. Temporal evolution of plasmon number in the dipole mode of a nanorod cavity with a varying decay rate γ_{tot} and an emitter number of (a) 3000 and (c) 1×10^5. A Gaussian pump pulse is launched at 3 ps with a width of 1 ps. The color bar shows the plasmon number in the dipole lasing mode. (b) Temporal evolution of plasmon number (blue solid curve) and population inversion (orange dashed curve) in the four typical cases in (a) with γ_{tot} of (i) 1×10^{10} s^{-1}, (ii) 3.2×10^{11} s^{-1}, (iii) 3.2×10^{12} s^{-1}, and (iv) 3.2×10^{14} s^{-1}. (d) Temporal evolution of plasmon number and population inversion in the four typical cases in (c) with γ_{tot} of (i) 1×10^9 s^{-1}, (ii) 1×10^{10} s^{-1}, (iii) 1×10^{12} s^{-1}, and (iv) 3.2×10^{14} s^{-1}. For reference, the pulse profile is given in the top column.

which in turn offers a gain large enough to compensate the cavity loss, and establishes lasing oscillation with feedback from the dipole-mode plasmons. Upon the pump pulse, n increases rapidly to a peak value of 11 and fades out afterward. When n decreases to 1 at $\sim$5 ps, the lasing condition ceases due to insufficient gain.

(iii) When γ_{tot} is further increased to, e.g., 3.2×10^{12} s^{-1}, corresponding to $F_P = 3.2 \times 10^4$, the decay rate from $L2$ to $L1$ is further increased, yielding a significantly reduced PIR (peak value of about 1.2%). However, PIR remains positive to ensure the lasing condition. Also, due to the large γ_{tot}, within the pump duration (e.g., 2–4 ps), the system is pumped to a state just slightly above the lasing threshold, and n simply evolves following the temporal profile of the pump pulse, with a peak value of 12 at 3.1 ps.

(iv) Finally, when γ_{tot} is increased to exceed the nonradiative interband transition rate 1×10^{13} s^{-1}, e.g., 3.2×10^{14} s^{-1}, corresponding to $F_P = 3.2 \times 10^6$, the population of $L2$ (N_2) is depleted much faster than that of $L1$ (N_1), and population inversion is no longer reachable. Therefore, throughout the process, the lasing threshold cannot be reached, with PIR remaining negative and $n < 1$.

It is clear that the Purcell effect (which can be very strong in a nanoplasmonic system, e.g., F_P as high as 1×10^4 [28]) plays an important role in establishing or destroying the lasing oscillation. For a given emitter, the spontaneous emission rate

can be modified within a large range proportional to F_P by coupling the emitter to a nanoplasmonic cavity mode. As seen in case (i) in Fig. 3(a), when γ_{tot} is 1×10^{10} s^{-1}, which is 100 times larger than that of a typical emitter without Purcell enhancement, e.g., 1×10^8 s^{-1} in a SiO$_2$ substrate [10,11], it is still too low to strengthen the stimulated emission toward lasing oscillation. Thus, to reach the lasing condition, a very large F_P is required. As seen in case (ii), only when γ_{tot} is increased to a level high enough, e.g., 3.2×10^{11} s^{-1}, can the significantly enhanced stimulated emission offer sufficient gain to compensate the cavity loss and build up the lasing oscillation. On the other hand, from stage (iii) to (iv), when γ_{tot} is increased to exceed the nonradiative interband transition rate of the gain material, the population at the upper lasing level ($L2$) will be depleted too fast to reach population inversion, and no lasing oscillation will occur in this case.

It is worth mentioning here that the available emitter number is also engineerable and important for lasing oscillation. Figures 3(c) and 3(d) show the calculated results of the nanolaser system with the same geometry but an emitter number of $N_{tot} = 1 \times 10^5$. Compared with that in Figs. 3(a) and 3(b), the increase in N_{tot} greatly facilitates the buildup of lasing oscillation under relatively lower γ_{tot}. For example, the onset point in this case [Fig. 3(c)] decreases to $\gamma_{tot} = 1.6 \times 10^9$ s^{-1}, much lower than that ($\gamma_{tot} = 6.3 \times 10^{10}$ s^{-1}) in Fig. 3(a). Also, a pronounced lasing oscillation is observed in case (ii) [Figs. 3(c) and 3(d)] with $\gamma_{tot} = 1 \times 10^{10}$ s^{-1}, with a much larger peak value of n (up to 575). Therefore, the increase of N_{tot} may greatly alleviate the requirement on γ_{tot} (or, equivalently, the Purcell enhancement and the corresponding pumping intensity). However, practically, N_{tot} is limited by the volume of the gain material (determined by the effective near-field volume of the nanorod dipole mode) and the doping concentration (without an evident quenching effect). Note that here we have assumed an ideal gain medium with the same emitter decay rate and β factor and changed the overall parameter γ_{tot} to roughly illustrate the influence of the Purcell effect on lasing behavior. Practical guidance for experimental implementation should consider both the position and orientation dependences of the emitter-nanoparticle coupling behavior, which is included in the next section.

C. Single-nanorod plasmon laser: Practical configuration

For a practical configuration, we consider a plasmon laser composed of a Au nanorod with a 14-nm diameter d and different lengths L, wrapped with a 15-nm-thick layer of SiO$_2$ consisting of a 1-nm emitter-free spacer layer near the nanorod surface and a 14-nm-thick gain medium (see Fig. 1). The total emitter number N_{tot} is assumed to be 4500, corresponding to the same emitter concentration of 174 mmol/L as that in a nanosphere system reported in a previous work [10].

To account for position and orientation dependences of emitters, we calculate random cases and sum them up to obtain an average value with high convergence (see Appendix B). The calculated plasmon number n in the dipole mode in the steady state with increasing pump rate is given in Fig. 4(a); for reference, n in a nanosphere system is also provided. It should be mentioned that, in a nanoplasmonic lasing system with $\beta \sim 1$, the conventional criterion for the
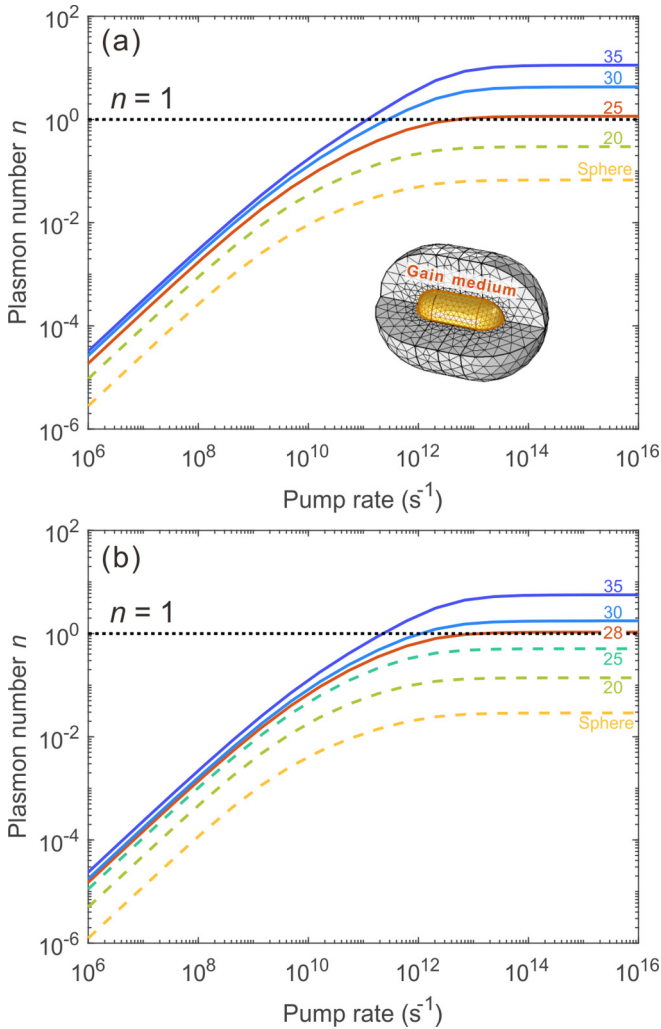
FIG. 4. Steady-state plasmon number in the lasing mode in Au nanorods with different lengths. (a) The emitter number for all cases is 4500. (b) The emitter concentration for all cases is 78 mmol/L (corresponding to a nanosphere with an emitter number of 2000 or a 28-nm-length nanorod with an emitter number of 2870). The length of each nanorod is labeled next to the corresponding curve in nanometers. The dotted line indicates the threshold of lasing. The inset in (a) shows the gain medium layer, which is divided by a small tetrahedron generated in the finite element method (FEM)-based quasinormal mode analysis, in order to consider the position-dependent emitter decay rate.

laser threshold, either the kink in the linear coordinate or the S curve in the log-log coordinate [29,30], is absent, resulting in a seemingly "thresholdless" lasing behavior [30]. In such cases, a more rigorous criterion is to examine the photon (plasmon) statistics regarding the degree of second-order coherence [31] and to define the threshold when the stimulated emission rate begins to surpass the spontaneous emission rate, which is semiclassically equivalent to equal emission rates of spontaneous and stimulated processes when the cavity plasmon number n is 1 [10,32], as denoted by the dotted line in Fig. 4.

It is clearly seen that, for a nanosphere, no matter how large the pump rate is, n remains much lower than 1 (e.g., saturated at about 0.07 with pump rate $>1 \times 10^{13}$ s^{-1}) and therefore

far from reaching the lasing condition due to the high cavity loss, large fractional dissipation via the high-order mode, and relatively low β. When the nanoparticle is elongated along one dimension into a nanorod, n increases obviously, owing to the increased cavity Q factor (equivalently, the lower cavity loss), suppressed high-order mode dissipation, and, especially, increased Purcell enhancement of the gain and a closer-to-unity β. When L is increased to 25 nm, n reaches 1 with a pump rate of $\sim 5.3 \times 10^{12}$ s^{-1}, presenting an opportunity to realize a plasmon laser using a nanorod with a diameter of 14 nm and $L = 25$ nm, whose dipole-mode cavity volume (see Appendix C for details) is only 1.3 times that of a 14-nm-diameter nanosphere. Further increasing L can greatly reduce the lasing threshold; for example, the threshold pump rate for a 30-nm-long nanorod is 2.7×10^{11} s^{-1}, which is beneficial for reducing the thermal effect in these high-loss, ultracompact devices [3,33]. As a result of the large Purcell-enhanced gain and significantly suppressed high-order mode dissipation, it is also possible to implement a dipole-mode plasmon laser in a nanorod system with much smaller N_{tot} (i.e., much lower molecular concentration), which may be desired to eliminate possible fluorescence quenching in practical applications. For reference, Fig. 4(b) gives the calculated n of the dipole mode with an emitter concentration of 78 mmol/L, corresponding to $N_{tot} = 2000$ in a nanosphere plasmon laser with a particle diameter of 14 nm. Figure 4(b) shows that the lasing condition can be reached when elongating the nanorod to a length of 28 nm with the same emitter concentration, together with a higher pumping rate ($\sim 6.9 \times 10^{12}$ s^{-1}), which is critical to support the Purcell-enhanced stimulated emission rate with a large F_P (e.g., $F_P = 1643$ at $d = 5$ nm from the apex of the nanorod).

IV. CONCLUSION

In conclusion, we have proposed an experimentally feasible approach to realize plasmon lasers based on a single nanorod with 3D ultratight optical confinement. We show that, with available experimental conditions (e.g., pump technique and pump rate) and accessible material parameters of metals and gain media, it is possible to implement a dipole-mode single-nanoparticle plasmon laser by taking advantage of the following merits of a single-nanorod system: (1) larger Purcell enhancement of the gain, (2) efficient suppression of high-order-mode energy dissipation and a β factor increasing to near unity, (3) a higher cavity Q factor, and (4) a larger near-field volume for coupling more gain molecules. Our theoretical approach can be readily adapted to many other plasmonic nanolasing systems with high F_P, such as bowtie resonators [34] and nanoparticle-on-mirror gap plasmon resonators [35]. We believe that the nanorod lasing system we have demonstrated will pave the way toward unprecedented plasmon lasers with ultratight optical confinement in all three dimensions and open opportunities for a variety of nanophotonic techniques based on 3D ultraconfined lasing modes.
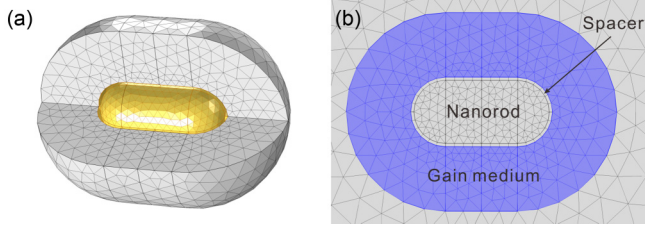
FIG. 5. (a) Tetrahedron mesh in the gain medium in the FEM calculation. (b) Cross section of the mesh region.

APPENDIX A: DRUDE MODEL FOR THE PERMITTIVITY OF GOLD NANOPARTICLES

To calculate the quasinormal modes of a gold nanoparticle, we use the Drude-Lorentz model to describe the permittivity of gold as

$$\varepsilon = \varepsilon_\infty \left[1 - \frac{\omega_{p,1}^2}{\omega^2 + i\omega\gamma_1} - \frac{\omega_{p,2}^2}{\omega^2 - \omega_{0,2}^2 + i\omega\gamma_2} \right], \quad (A1)$$

where $\varepsilon_\infty = 6$, $\omega_{p,1} = 5.37 \times 10^{15}$ s^{-1}, $\gamma_1 = 6.216 \times 10^{13}$, $\omega_{p,2} = 2.2636 \times 10^{15}$ s^{-1}, $\omega_{0,2} = 4.572 \times 10^{15}$ s^{-1}, $\gamma_2 = 1.332 \times 10^{15}$ s^{-1} [21]. The first two terms are the classical Drude model, and the third Lorentz term is employed to characterize the interband transitions of electrons, which start to contribute significantly at wavelengths shorter than 600 nm.

APPENDIX B: CALCULATION OF PLASMON NUMBER n

To account for position-dependent γ_m and β of emitters in the gain region induced by the large LSPR field gradient, we use the tetrahedron mesh in the FEM-based quasinormal mode analysis to separate the gain region into small tetrahedra, as shown in Fig. 5. In each tetrahedron, the electric field can be considered uniform due to the very small size of tetrahedron elements (the minimal element size is 2 nm, and element growth rate is 1.2 in the region of the gain medium), and the electric field is evaluated at the Gauss point of the tetrahedron element. In each mesh element, it is reasonable to assume all the emitters have the same orientation of dipole moments since the volume of each element is small. We generate randomly oriented dipole moment in all mesh elements in the gain region and calculate the corresponding emitter decay rate.

The evolution of carrier population is evaluated in each tiny tetrahedron region, and the contribution of all tetrahedron elements are combined to describe the evolution of the plasmon number in the dipole lasing mode as

$$\frac{dn}{dt} = \sum_j N_2^j \gamma_1^j + \sum_j \left(N_2^j - N_1^j \right) \gamma_1^j n - n\omega/Q,$$

$$\frac{dN_0^j}{dt} = \left(N_3^j - N_0^j \right) \gamma_P + N_1^j \gamma_{10},$$
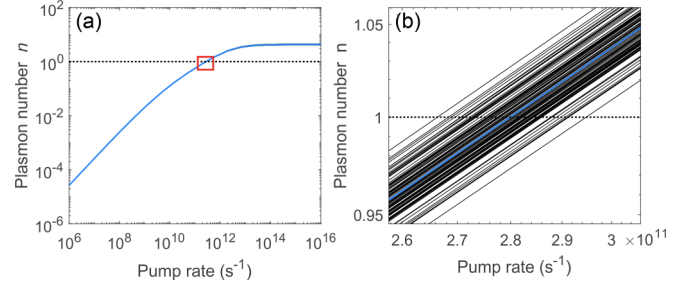

FIG. 6. Calculation of the averaged steady-state plasmon number. (a) The steady-state input-output curves of 30-nm-length nanorods with 100 different random distributions of emitter dipole orientation. The black dotted curve corresponds to one plasmon nanolaser with one certain dipole moment randomness. The blue solid curve shows the averaged steady-state input-output curve. (b) An enlarged view of the red rectangle region in (a).

$$\frac{dN_1^j}{dt} = \left(N_2^j - N_1^j \right) \gamma_1^j n + N_2^j \gamma_{tot}^j - N_1^j \gamma_{10}, \quad (B1)$$

$$\frac{dN_2^j}{dt} = \left(N_1^j - N_2^j \right) \gamma_1^j n - N_2^j \gamma_{tot}^j + N_3^j \gamma_{32},$$

$$\frac{dN_3^j}{dt} = \left(N_0^j - N_3^j \right) \gamma_P - N_3^j \gamma_{32},$$

where the emitter number in the jth tetrahedron is $N^j = \sum_{i=0}^3 N_i^j = \rho V_{tet}^j$, with ρ and V_{tet}^j being the emitter density and the volume of jth mesh element. Other parameters are the same as in Eq. (3). It should be noted that the dipole mode in a nanosphere has a threefold degeneracy which is different from that in a nanorod [10]. For each nanoparticle shape, we totally calculate 100 steady-state curves of the plasmon laser with different randomly generated distributions of emitters' dipole moments and average them to get the final steady-state curve (see Fig. 6 for an example).

For a typical case, when the nanorod has a length of 30 nm and a radius of 7 nm, the total number of mesh elements in the gain region is 19 032, indicating the total equation number in Eq. (B1) is 76 129. The Jacobian matrix of Eq. (B1) should be provided to speed up the numerical calculation.

APPENDIX C: CALCULATION OF THE LSPR MODE VOLUME

The energy density of the LSPR mode [35] in the nanoparticle is defined as

$$W(\mathbf{r}, \omega) = \frac{1}{2} \left(\frac{\partial[\omega\varepsilon(\mathbf{r}, \omega)]}{\partial\omega} \varepsilon_0 |\mathbf{E}_m(\mathbf{r}, \omega)|^2 + \mu_0 |\mathbf{H}_m(\mathbf{r}, \omega)|^2 \right), \quad (C1)$$

where $\varepsilon(\mathbf{r}, \omega)$ is the permittivity at position $\mathbf{r}$. The mode volume can be calculated as

$$V(\omega) = \frac{\int W(\mathbf{r}, \omega) d^3 \mathbf{r}}{\max[W(\mathbf{r}, \omega)]}, \quad (C2)$$

where the integration is performed in the whole calculation region of the FEM-based eigenfrequency analysis.

Figure 7 shows the mode volume of a nanorod as a function of the nanorod length. The dipole mode volume of a
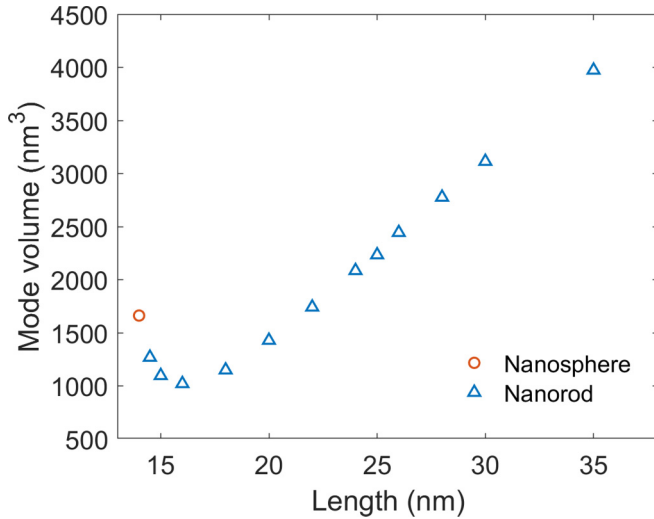
FIG. 7. Mode volume of the dipole mode in a nanosphere and nanorods with different lengths. The radii of all nanoparticles are 7 nm.

FIG. 8. A nanorod plasmon laser pumped by a 532-nm Gaussian beam with a diameter of w.

nanosphere with a radius of 7 nm is 1662 nm^3, while for a nanorod with the same radius and a length of 25 nm, the mode volume is 2234 nm^3, which is 1.3 times that of a nanosphere.

APPENDIX D: CALCULATION OF AVERAGE PUMP POWER

We assume that the fluorescent molecules considered in this work have an absorption cross section of 1×10^{-16} cm^2 [36], which is reasonable considering that the absorption cross section σ_{abs} of a typical fluorescent molecule is, e.g., 2.55×10^{-16} cm^2 for OG-488 [11] and 4×10^{-16} cm^2 for rhodamine 6G [23]. With a pump efficiency η of 80% and

a pump rate γ_p of 1×10^{12} s^{-1}, the corresponding peak pump intensity I_{peak} at a 532-nm wavelength can be obtained as $I_{peak} = hc\gamma_p/(\lambda_p \eta \sigma_{abs}) = 4.67$ GW/cm^2. When the pump beam has a Gaussian profile with a diameter of 10 μm (an experimentally reasonable spot size), the pump pulses are also Gaussian in the time domain with a duration or full width at half maximum (FWHM) of 1 ps for each pulse, as depicted in Fig. 8. One pulse could be described as

$$I(r, t) = \frac{P_{peak}}{\pi w^2/2} \exp\left(-2\frac{r^2}{w^2}\right) \exp\left(-4\ln 2\frac{t^2}{\tau^2}\right), \quad (D1)$$

where P_{peak} is the peak power, w is the beam radius, and τ is the FWHM of one pulse. Then, the calculated energy per pulse is 1.95 nJ, and with a repetition rate of 1 kHz, the average pump power is about 1.95 μW within the 10-m-size focusing spot or 0.11 nW on the cross section of a nanolaser consisting of a 14-nm-diameter 30-nm-long nanorod core and a 15-nm-thick gain coating layer (see also Fig. 1 for the structural configuration).

[1] D. J. Bergman and M. I. Stockman, Surface Plasmon Amplification by Stimulated Emission of Radiation: Quantum Generation of Coherent Surface Plasmons in Nanosystems, Phys. Rev. Lett. **90**, 027402 (2003).

[2] J. A. Schuller, E. S. Barnard, W. Cai, Y. C. Jun, J. S. White, and M. L. Brongersma, Plasmonics for extreme light concentration and manipulation, Nat. Mater. **9**, 193 (2010).

[3] R. M. Ma and R. F. Oulton, Applications of nanolasers, Nat. Nanotechnol. **14**, 12 (2019).

[4] E. Bermudez-Urena, G. Tutuncuoglu, J. Cuerda, C. L. Smith, J. Bravo-Abad, S. I. Bozhevolnyi, I. M. A. Fontcuberta, F. J. Garcia-Vidal, and R. Quidant, Plasmonic waveguide-integrated nanowire laser, Nano Lett. **17**, 747 (2017).

[5] R. M. Ma, R. F. Oulton, V. J. Sorger, G. Bartal, and X. Zhang, Room-temperature sub-diffraction-limited plasmon laser by total internal reflection, Nat. Mater. **10**, 110 (2011).

[6] T. P. H. Sidiropoulos, R. Röder, S. Geburt, O. Hess, S. A. Maier, C. Ronning, and R. F. Oulton, Ultrafast plasmonic nanowire lasers near the surface plasmon frequency, Nat. Phys. **10**, 870 (2014).

[7] R. F. Oulton, V. J. Sorger, T. Zentgraf, R. M. Ma, C. Gladden, L. Dai, G. Bartal, and X. Zhang, Plasmon lasers at deep subwavelength scale, Nature (London) **461**, 629 (2009).

[8] H. Wu, Y. Gao, P. Xu, X. Guo, P. Wang, D. Dai, and L. Tong, Plasmonic nanolasers: Pursuing extreme lasing conditions on nanoscale, Adv. Opt. Mater. **7**, 1900334 (2019).

[9] I. E. Protsenko, A. V. Uskov, O. A. Zaimidoroga, V. N. Samoilov, and E. P. O'Reilly, Dipole nanolaser, Phys. Rev. A **71**, 063812 (2005).

[10] G. Kewes, K. Herrmann, R. Rodriguez-Oliveros, A. Kuhlicke, O. Benson, and K. Busch, Limitations of Particle-Based Spasers, Phys. Rev. Lett. **118**, 237402 (2017).

[11] M. A. Noginov, G. Zhu, A. M. Belgrave, R. Bakker, V. M. Shalaev, E. E. Narimanov, S. Stout, E. Herz, T. Suteewong, and U. Wiesner, Demonstration of a spaser-based nanolaser, Nature (London) **460**, 1110 (2009).

[12] X. Meng, A. V. Kildishev, K. Fujita, K. Tanaka, and V. M. Shalaev, Wavelength-tunable spasing in the visible, Nano Lett. **13**, 4106 (2013).

[13] Z. Wang, X. Meng, A. V. Kildishev, A. Boltasseva, and V. M. Shalaev, Nanolasers enabled by metallic nanoparticles: From spasers to random lasers, Laser Photonics Rev. **11**, 1700212 (2017).

[14] N. Arnold, C. Hrelescu, and T. A. Klar, Minimal spaser threshold within electrodynamic framework: Shape, size and modes, Ann. Phys. (Berlin, Ger.) **528**, 295 (2016).

[15] X.-L. Zhong and Z.-Y. Li, All-analytical semiclassical theory of spaser performance in a plasmonic nanocavity, Phys. Rev. B **88**, 085101 (2013).

[16] X. F. Li and S. F. Yu, Design of low-threshold compact Au-nanoparticle lasers, Opt. Lett. **35**, 2535 (2010).

[17] J. B. Khurgin and G. Sun, Injection pumped single mode surface plasmon generators: Threshold, linewidth, and coherence, Opt. Express **20**, 15309 (2012).

[18] S.-Y. Liu, J. Li, F. Zhou, L. Gan, and Z.-Y. Li, Efficient surface plasmon amplification from gain-assisted gold nanorods, Opt. Lett. **36**, 1296 (2011).

[19] P. Anger, P. Bharadwaj, and L. Novotny, Enhancement and Quenching of Single-Molecule Fluorescence, Phys. Rev. Lett. **96**, 113002 (2006).

[20] L. Novotny and B. Hecht, *Principles of Nano-optics* (Cambridge University Press, Cambridge, 2006).

[21] W. Yan, R. Faggiani, and P. Lalanne, Rigorous modal analysis of plasmonic nanoresonators, Phys. Rev. B **97**, 205422 (2018).

[22] C. Ciraci, R. T. Hill, J. J. Mock, Y. Urzhumov, A. I. Fernandez-Dominguez, S. A. Maier, J. B. Pendry, A. Chilkoti, and D. R. Smith, Probing the ultimate limits of plasmonic enhancement, Science **337**, 1072 (2012).

[23] J. R. Lakowicz, *Principles of Fluorescence Spectroscopy* (Springer, Boston, MA, 2013).

[24] R. Ruppin, Decay of an excited molecule near a small metal sphere, J. Chem. Phys. **76**, 1681 (1982).

[25] N. Gregersen, T. Suhr, M. Lorke, and J. Mørk, Quantum-dot nano-cavity lasers with Purcell-enhanced stimulated emission, Appl. Phys. Lett. **100**, 131107 (2012).

[26] A. J. Campillo, J. D. Eversole, and H. B. Lin, Cavity Quantum Electrodynamic Enhancement of Stimulated Emission in Microdroplets, Phys. Rev. Lett. **67**, 437 (1991).

[27] B. Romeira and A. Fiore, Purcell effect in the stimulated and spontaneous emission rates of nanoscale semiconductor lasers, IEEE J Quantum Electron. **54**, 2000412 (2018).

[28] G. M. Akselrod, C. Argyropoulos, T. B. Hoang, C. Ciracì, C. Fang, J. Huang, D. R. Smith, and M. H. Mikkelsen, Probing the mechanisms of large Purcell enhancement in plasmonic nanoantennas, Nat. Photonics **8**, 835 (2014).

[29] S. H. Pan, Q. Gu, A. El Amili, F. Vallini, and Y. Fainman, Dynamic hysteresis in a coherent high-β nanolaser, Optica **3**, 1260 (2016).

[30] M. Khajavikhan, A. Simic, M. Katz, J. H. Lee, B. Slutsky, A. Mizrahi, V. Lomakin, and Y. Fainman, Thresholdless nanoscale coaxial lasers, Nature (London) **482**, 204 (2012).

[31] Y. J. Lu, J. Kim, H. Y. Chen, C. Wu, N. Dabidian, C. E. Sanders, C. Y. Wang, M. Y. Lu, B. H. Li, X. Qiu, W. H. Chang, L. J. Chen, G. Shvets, C. K. Shih, and S. Gwo, Plasmonic nanolaser using epitaxially grown silver film, Science **337**, 450 (2012).

[32] G. Bjork, A. Karlsson, and Y. Yamamoto, Definition of a laser threshold, Phys. Rev. A **50**, 1675 (1994).

[33] K. Ding and C. Z. Ning, Metallic subwavelength-cavity semiconductor nanolasers, Light Sci. Appl. **1**, e20 (2012).

[34] J. Y. Suh, C. H. Kim, W. Zhou, M. D. Huntington, D. T. Co, M. R. Wasielewski, and T. W. Odom, Plasmonic bowtie nanolaser arrays, Nano Lett. **12**, 5769 (2012).

[35] R. Chikkaraddy, B. de Nijs, F. Benz, S. J. Barrow, O. A. Scherman, E. Rosta, A. Demetriadou, P. Fox, O. Hess, and J. J. Baumberg, Single-molecule strong coupling at room temperature in plasmonic nanocavities, Nature (London) **535**, 127 (2016).

[36] L. Kastrup and S. W. Hell, Absolute optical cross section of individual fluorescent molecules, Angew. Chem., Int. Ed. **43**, 6646 (2004).